# REPORT DOCUMENTATION PAGE

*Form Approved*
*OMB No. 0704-0188*



| 1. REPORT DATE *(DD-MM-YYYY)* | 2. REPORT TYPE | 3. DATES COVERED *(From - To)* |
|---|---|---|
| 28-07-2009 | Conference Proceeding | |

**4. TITLE AND SUBTITLE**
Global High Resolution Analyses and Forecasts at the Mesoscale

**5a. CONTRACT NUMBER**

**5b. GRANT NUMBER**

**5c. PROGRAM ELEMENT NUMBER**
0601153N

**6. AUTHOR(S)**
Harley E. Hurlburt, Y. Drillet, G. Brassington, M. Benkiran, Eric Chassignet, James A. Cummings, M. Drevillon, H. Etienne, O. Le Galloudec, E. Joseph Metzger, P. Oke, T. Pugh, A. Schiller, Jay Shriver, Ole Martin Smedstad, B. Tranchant, Alan J. Wallcraft, G. Warren

**5d. PROJECT NUMBER**

**5e. TASK NUMBER**

**5f. WORK UNIT NUMBER**
73-8677-08-5

**7. PERFORMING ORGANIZATION NAME(S) AND ADDRESS(ES)**
Naval Research Laboratory
Oceanography Division
Stennis Space Center, MS 39529-5004

**8. PERFORMING ORGANIZATION REPORT NUMBER**
NRL/PP/7304-08-9062

**9. SPONSORING/MONITORING AGENCY NAME(S) AND ADDRESS(ES)**
Office of Naval Research
800 N. Quincy St.
Arlington, VA 22217-5660

**10. SPONSOR/MONITOR'S ACRONYM(S)**
ONR

**11. SPONSOR/MONITOR'S REPORT NUMBER(S)**

**12. DISTRIBUTION/AVAILABILITY STATEMENT**
Approved for public release, distribution is unlimited.

**13. SUPPLEMENTARY NOTES**

20090805542

**14. ABSTRACT**
The feasibility of global ocean weather prediction was just emerging as GODAE began in 1997. Ocean weather includes phenomena such as meandering currents and fronts, eddies, the surface mixed layer and SST, equatorial and coastally trapped waves, upwelling of cold water, and Rossby waves, all influencing ocean variables such as temperature (T), salinity (S), currents, and sea surface height (SSH). Adequate realtime data input, computing power, numerical ocean models, data assimilation capabilities, atmospheric forcing, and bathymetric/boundary constraints are essential to make such prediction possible. The key observing systems and real-time data inputs are SSH from satellite altimetry, satellite and in situ SST, T or T&S profiles (e.g. ARGO, TAO, PIRATA, BTs), and atmospheric forcing. The results are substantially influenced by ocean model simulation skill and it is advantageous to use an ocean model that is eddy-resolving (typically < 8 km grid increments), not just eddy-permitting. Since the most abundant ocean observations are satellite surface data and subsurface data are very sparse in relation to the space scales of the mesoscale ocean features that dominate the ocean interior, downward projection of surface data is a key challenge in ocean data assimilation. The need for accurate prediction of ocean features that are inadequately observed, such as the mixed layer depth, places a major burden on the ocean model, the data assimilation, and the atmospheric forcing. Demonstrations of feasibility in relation to the preceding phenomena, requirements, and challenges will be drawn from the following global ocean prediction systems: BLUElink (Australia), HYCOM (USA), Mercator-Ocean (France), NCOM (USA), and NLOM (USA).

**15. SUBJECT TERMS**
global ocean prediction, mesoscale ocean prediction, operational ocean prediction, ocean forecast skil

| 16. SECURITY CLASSIFICATION OF: | | | 17. LIMITATION OF ABSTRACT | 18. NUMBER OF PAGES | 19a. NAME OF RESPONSIBLE PERSON |
|---|---|---|---|---|---|
| a. REPORT | b. ABSTRACT | c. THIS PAGE | | | Harley Hurlburt |
| Unclassified | Unclassified | Unclassified | UL | 17 | 19b. TELEPHONE NUMBER *(Include area code)* 228-688-4626 |

# 3.1 Global High Resolution Analyses and Forecasts at the Mesoscale

H. E. Hurlburt[1], Y. Drillet[2], G. B. Brassington[3], M. Benkiran[4], E. P. Chassignet[5], J. A. Cummings[6], M. Drevillon[7], H. Etienne[4], O. Le Galloudec[2], E. J. Metzger[1], P. R. Oke[8], T. Pugh[3], A. Schiller[8], J. F. Shriver[1], O. M. Smedstad[9], B. Tranchant[7], A. J. Wallcraft[1], G. Warren[10]

[1]*Naval Research Laboratory, Stennis Space Center, MS, USA*
[2]*Mercator-Océan, Ramonville Saint Agne, France*
[3]*Centre for Australian Weather and Climate Research, BoM, Melbourne, Australia*
[4]*CLS, Ramonville Saint Agne, France*
[5]*Florida State University, COAPS, Tallahassee, FL, USA*
[6]*Naval Research Laboratory, Monterey, CA, USA*
[7]*CERFACS, Toulouse, France*
[8]*Centre for Australian Weather and Climate Research, CSIRO, Hobart, Australia*
[9]*QinetiQ North America, TSG-PSI, Stennis Space Center, MS, USA*

**Abstract**

The feasibility of global ocean weather prediction was just emerging as GODAE began in 1997. Ocean weather includes phenomena such as meandering currents and fronts, eddies, the surface mixed layer and sea surface temperature (SST), equatorial and coastally trapped waves, upwelling of cold water, and Rossby waves, all influencing ocean variables such as temperature (T), salinity (S), currents, and sea surface height (SSH). Adequate real-time data input, computing power, numerical ocean models, data assimilation capabilities, atmospheric forcing, and bathymetric/boundary constraints are essential to make such prediction possible. The key observing systems and real-time data inputs are SSH from satellite altimetry, satellite and in situ SST, T or T&S profiles (e.g. Argo, TAO, PIRATA, BTs), and atmospheric forcing. The ocean models dynamically interpolate the data in conjunction with the data assimilation, convert atmospheric forcing into oceanic responses, and forecast the ocean weather, applying the bathymetric/boundary constraints in the process. The results are substantially influenced by ocean model simulation skill and it is advantageous to use an ocean model that is eddy-resolving (typically < 8 km grid increments), not just eddy-permitting. Since the most abundant ocean observations are satellite surface data and subsurface data are very sparse in relation to the space scales of the mesoscale ocean features that dominate the ocean interior, downward projection of surface data is a key challenge in ocean data assimilation. The need for accurate prediction of ocean features that are inadequately observed, such as the mixed layer depth, places a major burden on the ocean model, the data assimilation, and the atmospheric forcing. The sensitivity of ocean phenomena to the atmospheric forcing and the time scale for response affect the time scale for oceanic predictive skill, sensitivity to the initial state versus the atmospheric forcing as a function of forecast length, and thus oceanic data requirements and prediction system design. Outside surface boundary layers and shallow regions, forecast skill is ~1 month globally and over many subregions and is only modestly reduced by reverting toward climatological forcing after the end of the atmospheric forecasts versus using analysis-quality forcing for the duration. In addition, global ocean prediction systems must demonstrate the ability to provide initial and boundary conditions to nested regional and coastal models that enhance their predictive skill. Demonstrations of feasibility in relation to the preceding phenomena, requirements, and challenges are drawn from the following global ocean prediction systems: BLUElink (Australia), HYCOM (USA), Mercator Océan (France), NCOM (USA), and NLOM (USA).

**Key Words:** global ocean prediction, mesoscale ocean prediction, operational ocean prediction, ocean forecast skil

## 1. Introduction

At the beginning of the Global Ocean Data Assimilation Experiment (GODAE) in the late 1990s, the feasibility of global ocean prediction at the mesoscale was discussed primarily in terms of enabling technologies, topics discussed in Wilson et al. (2008, this volume), Harrison et al. (2008, this volume), and Dombrowsky et al. (2008, this volume). At the end of GODAE we can present demonstrations of feasibility based on the capabilities and limitations of present real-time operational and pre-operational GODAE ocean prediction systems, here for global high resolution nowcasts and forecasts at the mesoscale. We also include some indications of the potential for future increases in capability.

## 2. Need for an eddy-resolving ocean model

An eddy-resolving global ocean model is an essential component for global prediction at the mesoscale because of its roles in (1) dynamical interpolation of the data during data assimilation, (2) representing the poorly observed subsurface ocean, (3) converting atmospheric forcing into ocean responses, (4) accurately applying topographic/geometric constraints, (5) producing forecasts of the "ocean weather", and (6) providing boundary conditions and initial conditions for nested regional and coastal models with even higher resolution. A global comparison of sea surface height (SSH) variability from the model with SSH variability measured by satellite altimetry is a very useful step in assessing the ability of the model to represent mesoscale variability. Mesoscale variability is the leading deep water source of SSH variability retained in the altimetry maps outside the waveguides for equatorial and coastally-trapped waves. Figure 1 compares (a) SSH variability over 2004-2006 simulated by 1/12° Mercator Océan without data assimilation and (b) SSH variability calculated from weekly model-independent 1/3° analyses of sea level anomalies from satellite altimeter data, performed at the CLS Space Oceanography Division. The global pattern and amplitude of the variability simulated by the model is very similar to that from the altimetry, with an almost one-to-one correspondence between large and small features with high, intermediate and low variability. The success in simulating the variability associated with the Agulhas retroflection at the southern tip of Africa is particularly noteworthy because this has been a difficult feat for global ocean models. This comparison is clear evidence that the 1/12° Mercator Océan simulation is eddy-resolving. The variability is substantially higher and more realistic than from a corresponding 1/4° global Mercator Océan eddy-permitting simulation without data assimilation (not shown). See Hurlburt et al. (2008a,b) for discussions of the significant dynamical distinction between eddy-resolving and eddy-permitting ocean models. The SSH variability in the 1/12° Mercator Océan simulation actually tends to exceed to that in the altimetry map because of the lower spatial and temporal resolution used in producing the CLS map.

Even eddy-resolving ocean models exhibit significant discrepancies in simulating the ocean, e.g. excessively high SSH variability in the northern half of the South China Sea (~10-20°N, 110-120°E) in the 1/12° Mercator Océan simulation. The Gulf Stream is notoriously difficult to simulate (Bryan et al., 2007; Chassignet and Marshall, 2008). The 1/12° Mercator Océan simulation is no exception. The altimetry shows an area of low SSH variability immediately to the north of the Gulf Stream after it separates from the coast near 35.5°N, 75°W. East of 60°W the Gulf region in the altimetry shows a much broader (north-south) region of variability than the model. Since there is particular interest in nowcasting and forecasting the mesoscale variability in this challenging region, Figure 2 is a zoom into the Gulf Stream region. It provides a comparison of SSH variability from a 1/12° global simulation by the HYbrid Coordinate Ocean Model (HYCOM) (without ocean data assimilation) (Fig. 2a) with along-track SSH variability from satellite altimeters in 4 orbits (Fig. 2b). West of ~69°W the altimetry depicts a narrow band of high SSH variability along the Gulf Stream with very low variability north of the stream versus a broad area of high variability in the global 1/12° HYCOM and variability higher than observed on the north side of the Gulf Stream in both the 1/12° HYCOM and Mercator Océan simulations. See Hurlburt and Hogan (2008) for an explanation of the Gulf Stream pathway and related narrow band of high variability in this region, an explanation that is strongly supported by observational evidence. In the same region HYCOM exhibits a mean Gulf Stream pathway that is only slightly too far south and lies along the northern edge of a baroclinically unstable recirculation gyre with a narrow north-south extent (~2°) that is inconsistent with observational evidence. An eddy-driven mean abyssal gyre lies directly beneath the surface gyre centered over the northwesternmost relatively flat topography in the region. The HYCOM simulation does simulate the high variability associated with the Mann Eddy (~48-40°W, 40-46°N), but even though both 1/12° HYCOM and 1/12° Mercator Océan simulate

an eastern nonlinear recirculation gyre, both completely miss the high SSH variability that wraps around it in Figure 2b (~57-40°W, 35-41°N), a feature discussed in Hurlburt and Hogan (2000).

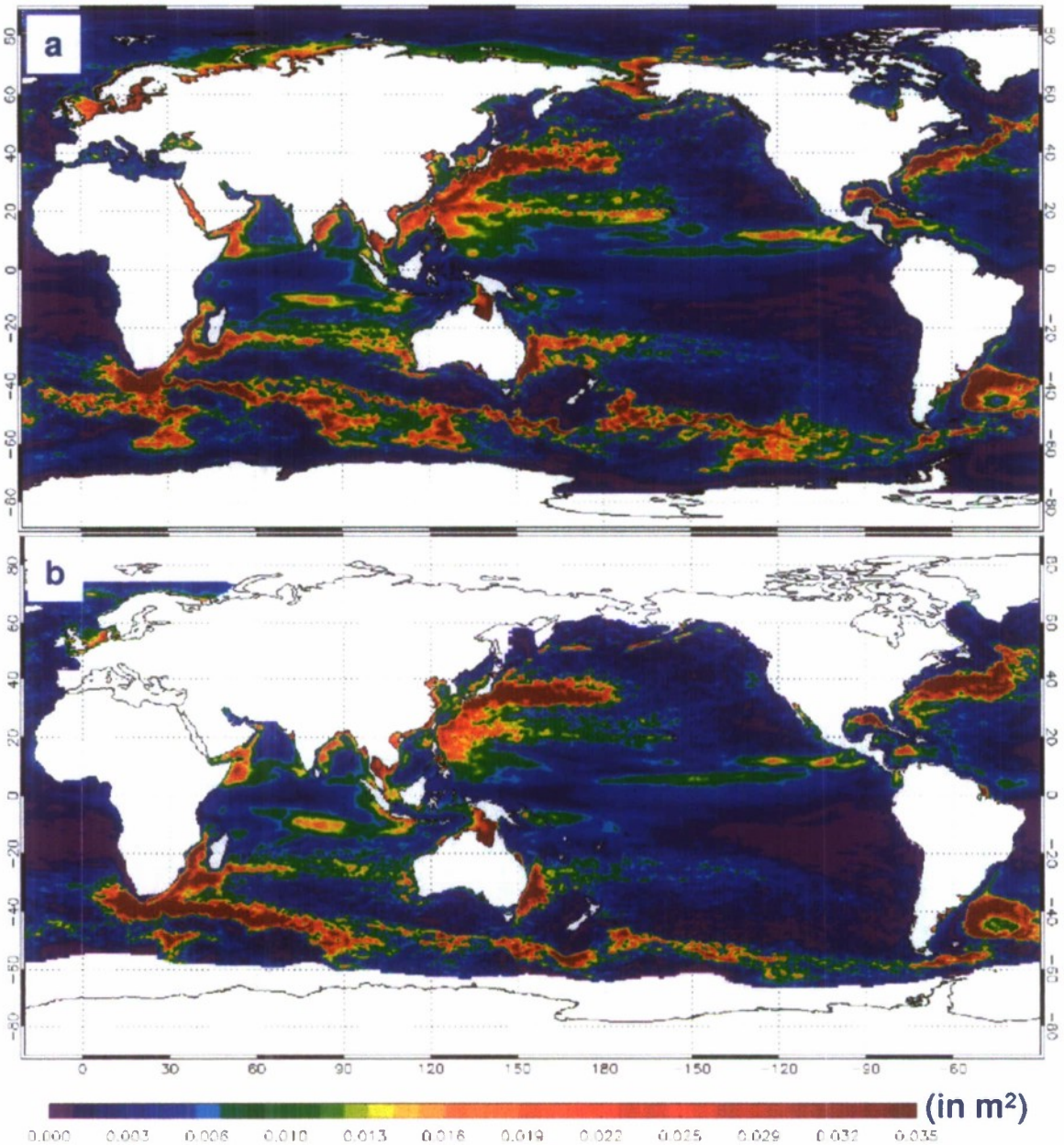


***Figure 1:*** *2004-2006 Sea Surface Height (SSH) variability ($m^2$) calculated (a) from the 1/12° global Mercator Océan configuration, ORCA12, run without ocean data assimilation and (b) from satellite altimeter data.*

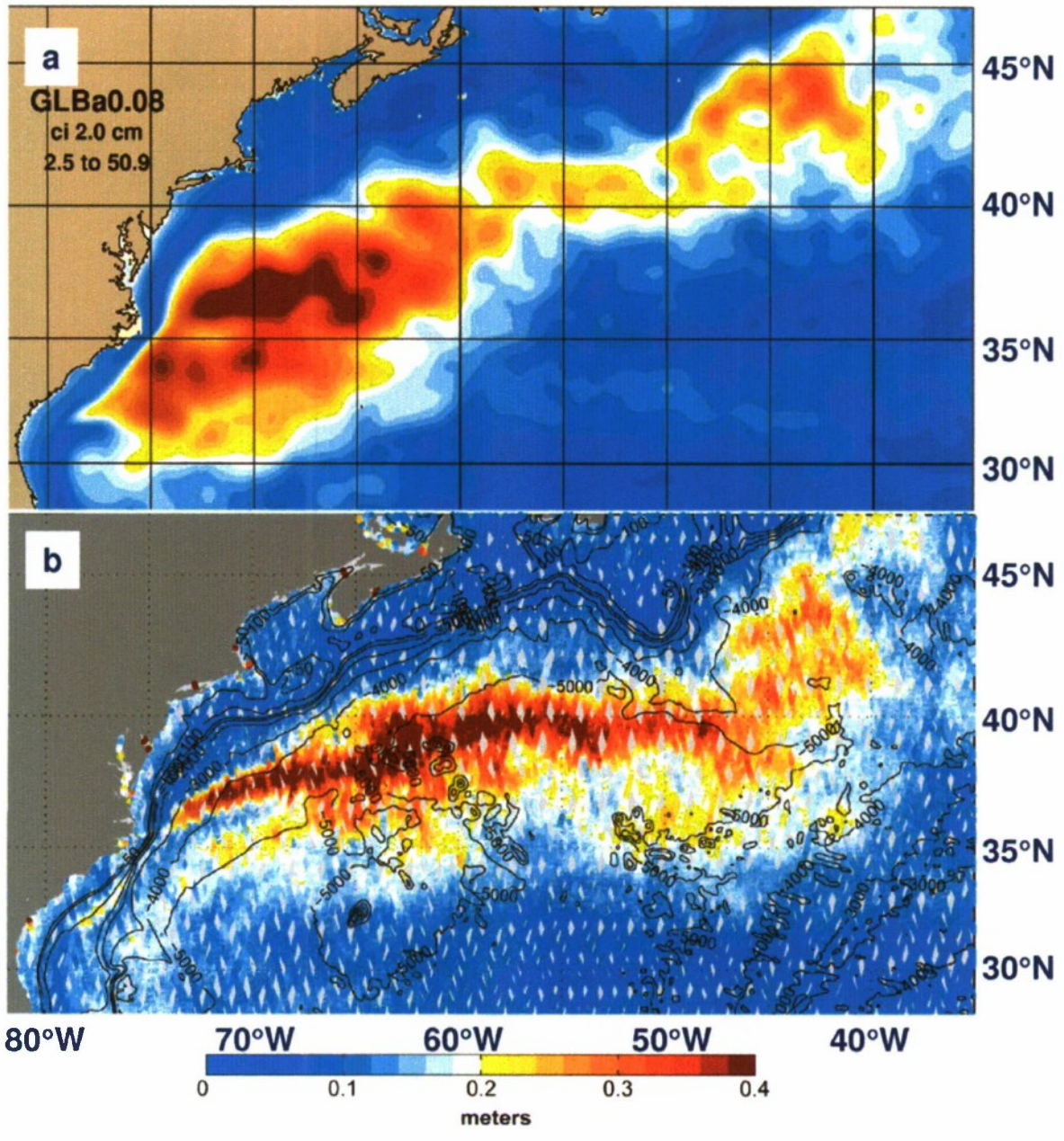


***Figure 2**: (a) Root Mean Square (RMS) SSH variability over four model years from a non-assimilative 1/12° global HYCOM simulation using climatological wind and thermal forcing from the European Centre for Medium-Range Weather Forecasts (ECMWF) with wind speed corrected using a QuikSCAT climatology. (b) Quasi-contemporaneous along-track RMS SSH variability from satellite altimeter data in four orbits overlaid on topographic contours (depth in m). The tracks are overlaid in the following order from top to bottom: (1) Envisat, (2) GFO, (3) Jason-1, and (4) Topex interleaved. (b) is from Hurlburt and Hogan (2008) and was provided by Gregg Jacobs, NRL.*

## 3. A ten day forecast demonstration for the Gulf Stream

Despite the shortcomings, the 1/12° global Mercator Océan and HYCOM simulations both exhibit quite realistic mean Gulf Stream pathways (not shown) that are consistent with the present state of the art for eddy-resolving ocean general circulation models (OGCMs) with high vertical resolution (Bryan et al., 2007; Chassignet and Marshall, 2008). In addition, significant progress has been made in nowcasting and forecasting the Gulf Stream as illustrated in Figure 3, where 10-day forecasts of current speed (at 92 m depth

for 26 April 2008) obtained from three different Mercator Océan prediction systems are compared with ocean color from MODIS. All three use the NEMO ocean model (Madec, 2008) and the SAM2 data assimilation scheme based on the SEEK filter (Brasseur and Verron, 2006), but in the 1/12° Atlantic and the 1/4° global the analysis correction is applied as a single increment at the analysis time, while the 1/12° global uses an incremental analysis update (IAU) applied over the week following the analysis date. See Dombrowsky et al. (2008 in this volume) for more information about the Mercator Océan and other prediction systems and Cummings et al. (2008 in this volume) for more information about the data assimilation in the different prediction systems.

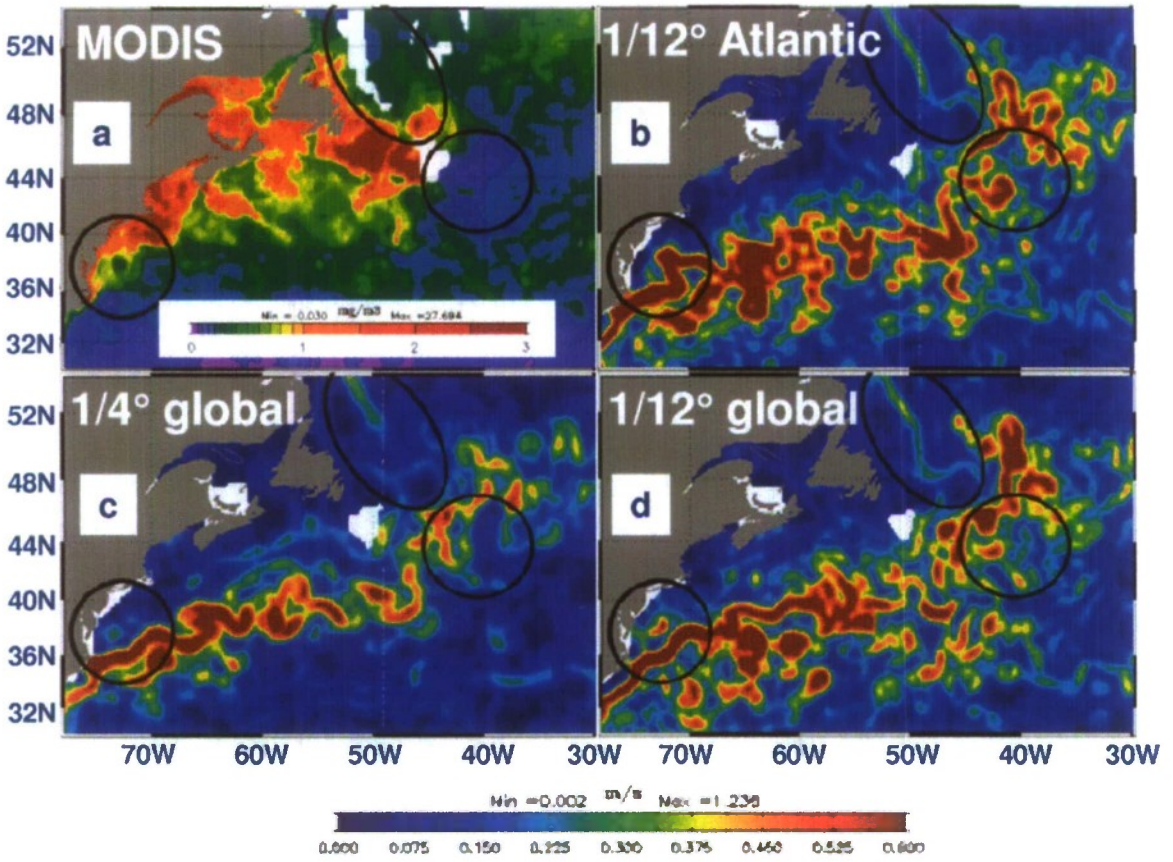


***Figure 3:*** *Chlorophyll-A concentration latest cloud-free pixel composite from MODIS for the week ending on 26 April 2008 (a) and ocean current forecasts at 92 meters depth on 26 April 2008 from three Mercator Océan prediction systems, (b) the 1/12° Atlantic and Mediterranean system, (c) the 1/4° global system, and (d) the 1/12° global system. Black circles illustrate some patterns.*

It is readily apparent that the 1/12° eddy-resolving systems depict much more mesoscale variability and smaller scale features than the 1/4° eddy-permitting system (Fig. 3b,c,d). In addition, the currents tend to be stronger in the 1/12° systems. In the MODIS ocean color (Fig. 3a) a strong eddy is depicted at the center of a circle (~38°N, 73°W) near the location where the Gulf Stream separates from the coast. This eddy is captured only in the 1/12° Atlantic system (a closed circulation is seen when current vectors are overlaid). All three of the systems depict currents around the high chlorophyll feature near 47°N within the southeastern end of the ellipse. In all three systems a current also flows along the boundary between green (moderate chlorophyll) and blue (low chlorophyll) all the way from a region just within the circle where it abuts the ellipse to a loop that extends northward just east of the ellipse. This associated current pathway is best depicted in the 1/4° global system. Thus, despite differences, evidence of 10-day forecast skill for specific features in the Gulf Stream region can be found in the Mercator Océan prediction systems by comparing the forecasts with the ocean color image.

## 4. Capability to nowcast mesoscale variability with real-time verification by drogued drifters

Another powerful means for visual verification of specific ocean features is illustrated in Figure 4.

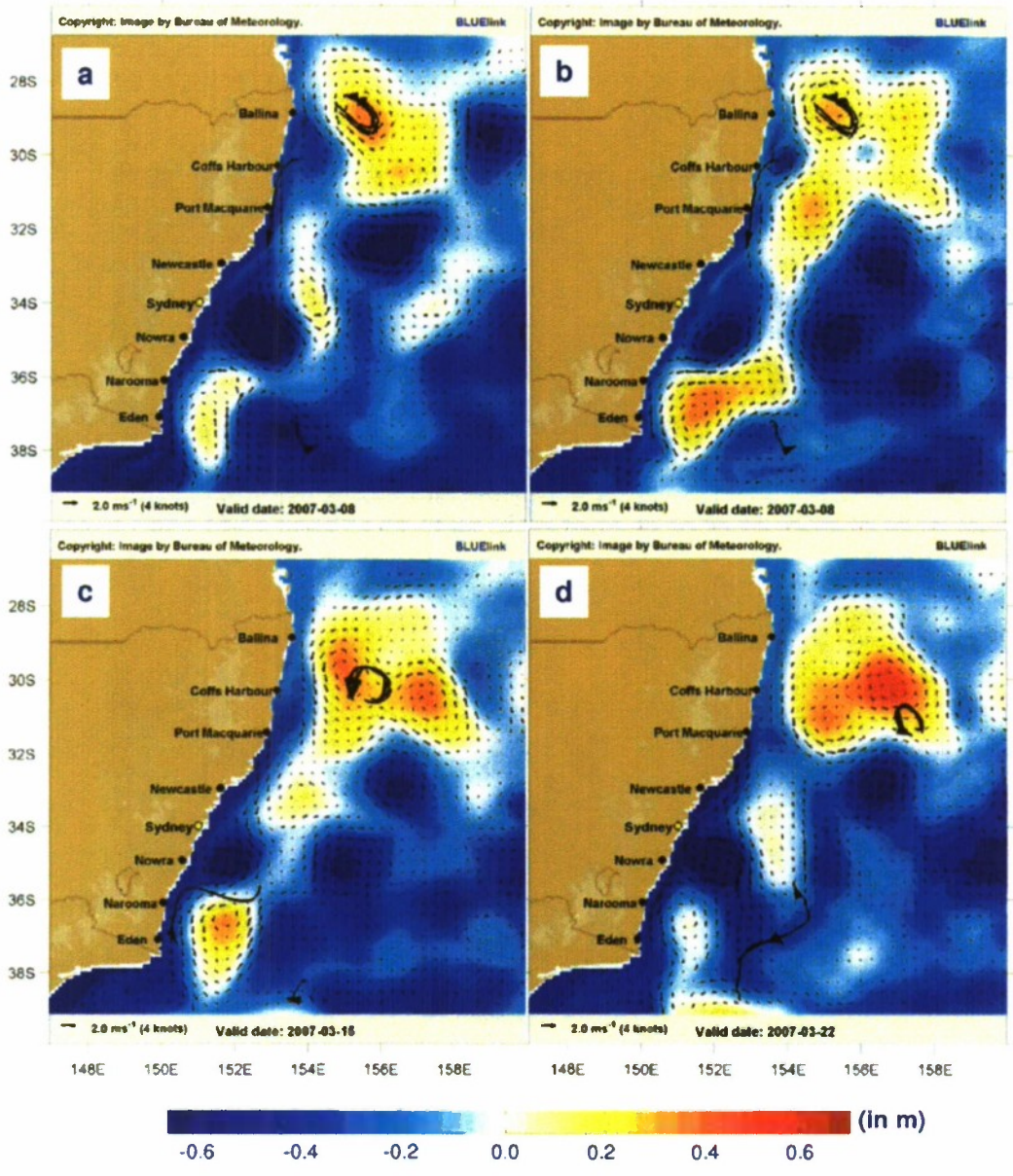


***Figure 4:*** *Snapshots of sea surface height (SSH) in the East Australia Current region with ocean current vectors and observed ± 2-day drifter trajectories overlaid. All are from the Australian BLUElink global ocean prediction system. This system has 1/10° resolution in the region around Australia (90°E-180°E, 75°S-16°N) and uses the ocean model MOM4 with multivariate EnOI data assimilation. (a) is from a reanalysis that uses data on both sides of the analysis date, while (b-d) are from the operational real-time system that only uses data up to the analysis date. (a) and (b) are for 8 Mar 2007, (c) for 15 March 2007, and (d) for 22 March 2007.*

Approximately 1250 drifters drogued at 15 m are deployed throughout the world ocean and report real-time data typically 16-20 times a day (Lumpkin and Pazos, 2007; NOAA, 2008). In Figure 4 four drifters in the East Australia Current system are used to evaluate the depiction of mesoscale variability in the Australian BLUElink prediction system, which is based on the ocean model MOM4 (Griffes et al., 2004) and the BLUElink ocean data assimilation system (BODAS) (Oke et al., 2008), a system that uses ensemble optimal interpolation (EnOI). The BLUElink system is global, but eddy-resolving (1/10°) only in a 90° sector surrounding Australia. Figure 4a and 4b are for the same date (8 March 2007). Figure 4a is from a reanalysis

that uses data on both sides of the analysis date, while Figure 4b is a nowcast that only uses data prior to the analysis time. Both depict generally similar mesoscale features, but with significant differences. Two of the drifters move in tandem for six weeks, here circling near the center of an anticyclonic eddy seen in both analyses. A third drifter is moving southward in the East Australia Current (EAC), again in general agreement with both analyses. Figure 4b, c, d depicts a sequence of nowcast states one week apart (b) 8 March 2007, (c) 15 March 2007, and (d) 22 March 2007. In Figure 4c and 4d the drifters traveling in tandem continue to circle an eddy that propagates offshore. The offshore propagation is not well captured in the nowcast. Instead it depicts a nearshore eddy that propagates southward and an offshore eddy that strengthens. The offshore propagation is better represented in the reanalysis (sequence not shown but represented for one date in Figure 4a). The drifter in the EAC continues rapidly southward during the first week and shows that the nowcast captures the cyclone/anticyclone pair along the coast between 34° and 38°S. In Figure 4d it returns toward the north followed by a fourth drifter that almost exactly overlays a trajectory segment of the third drifter. The reversal of the arrow on the fourth drifter trajectory indicates a tight loop before it subsequently moved toward the southeast. Since the drifter data are available in real time and the trajectory data are generally not assimilated by GODAE prediction systems, they represent an independent data set that can be routinely used for rapid assessment of mesoscale mapping by ocean prediction systems, especially the positioning of mesoscale eddies.

## 5. Capability to map small eddies (<75 km in diameter) using satellite altimetry and eddy-resolving global ocean prediction systems

Figure 5a presents an unusually clear SeaWiFS ocean color image that depicts a large number of eddies with a wide range of sizes from > 3° down to 1/4° in diameter. The eddies are numbered in order of decreasing size. Based on model-independent analyses of satellite altimeter data, Ducet et al. (2000) estimated 75 km as a lower bound for features that could be effectively mapped using satellite altimeter data. Here we investigate the ability of ocean model dynamical interpolation skill to extend that mapping to eddy diameters smaller than 75 km using results from three eddy-resolving and one eddy-permitting global ocean prediction systems (Fig. 5b-5e) and results from a simulation with atmospheric forcing but no ocean data assimilation (Figure 5f), the latter differing from Figure 5c only in the lack of ocean data assimilation. It is readily apparent that all of the data assimilative systems depict the four largest eddies, whereas the non-assimilative system does not.

Quantitative analyses are used to assess the ability of the different prediction systems to depict the large eddies (1-10, diameter $\geq$ 75 km) and small eddies (11-20, diameter (< 75 km) (summarized in Table 1). The data assimilative model with the finest resolution (4 km at 20°N) was able to depict the largest number of large and small eddies and gave the lowest eddy center location error. It clearly outperforms the same model without data assimilation in representing the small eddies. The eddy-resolving prediction systems with 8 km resolution also outperform the non-assimilative system in representing small eddies, but by a smaller margin. In contrast, the non-assimilative model outperforms the eddy-permitting prediction system (18 km resolution) in representing the small eddies. All of the data assimilative systems outperform the non-assimilative model in representing the large eddies. Generally, the systems are able to depict eddies that are at least 7 grid intervals in diameter, i.e. with a minimum diameter of 1/4°, 1/2°, and 1-1/4° for the prediction systems with 4 km, 8 km, and 18 km resolution at 20°N, respectively. In some cases the prediction systems map eddies smaller than the minimum by depicting them as eddies larger than the minimum. These results clearly indicate that the dynamical interpolation skill of an eddy-resolving ocean model can extend skillful mapping of eddies to eddy diameters that are smaller than obtained using model-independent analyses of altimeter data. Further, the minimum diameter of eddies seen in the ocean color image that were mapped by the ocean prediction systems was limited by the model resolution, not by the altimeter data in these tests.

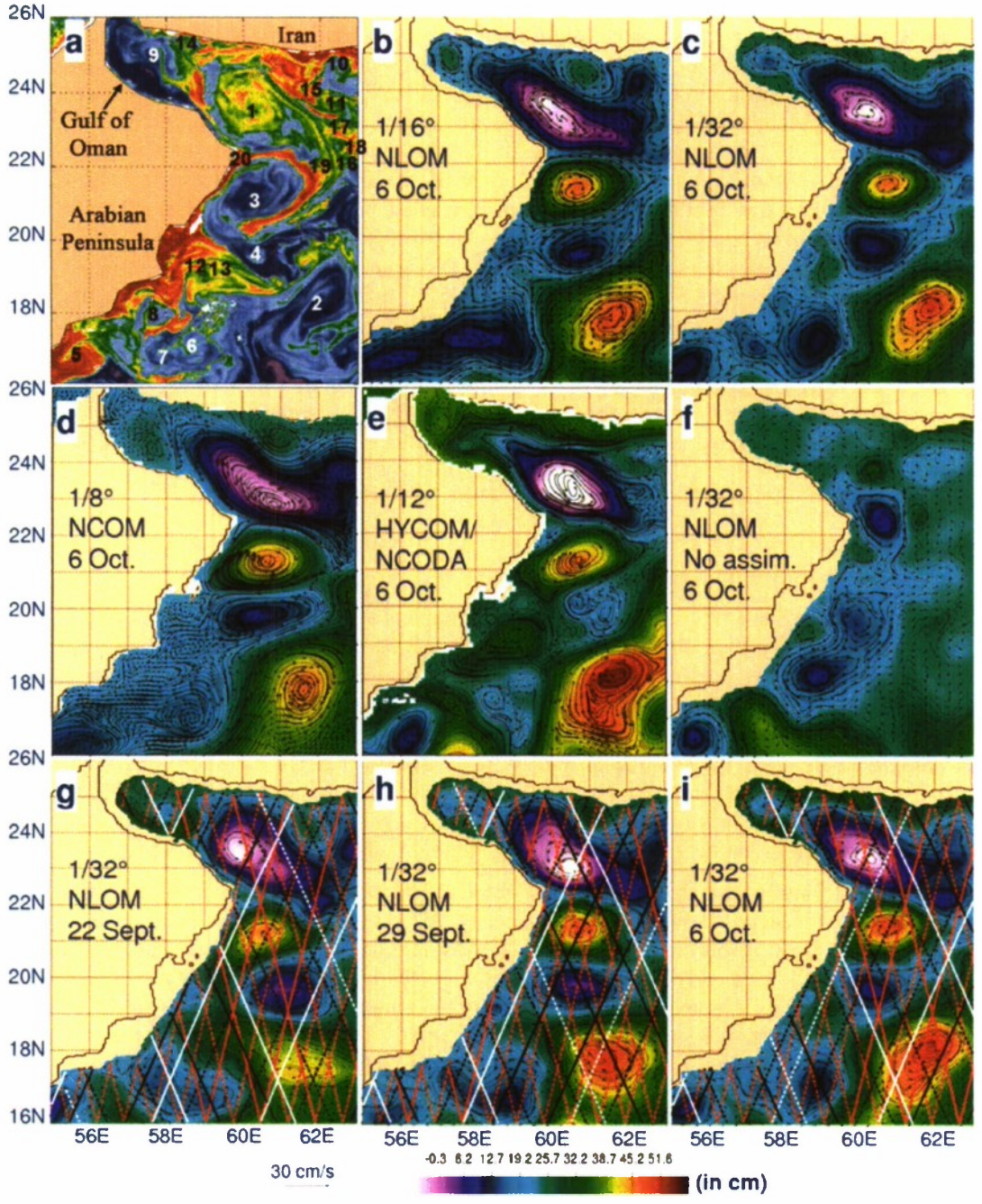


**Figure 5**: *Comparison of eddies and currents seen in (a) chlorophyll concentration from a SeaWiFS latest cloud-free pixel composite with most data from 6 Oct. 2002 with (b-e) data-assimilative model nowcast SSH and currents on 6 Oct. 2002 from (b) 1/16° global NLOM, (c) 1/32° global NLOM, (d) 1/8° global NCOM, and (e) 1/12° global HYCOM. (f ) same as (c) but without ocean data assimilation. In (a), eddies with clearly-defined eddy centers are numbered in order of decreasing size. Number color varies for visual clarity. 1/32° NLOM SSH and currents for (g) 22 Sept., (h) 29 Sept., and (i) 6 Oct. [same as (c)] with the most recent week of observed altimeter tracks overlaid as solid lines and the remaining tracks as dashed lines, red for ERS-2, black for GFO, and white for Jason-1. Jason-1 data were not yet used in the operational 1/16° NLOM system results in (b). A few of the smallest eddies are not visible due to the plot size or a model location east of 63°E. (Adapted from Hurlburt et al. (2008a) and Shriver et al. (2007)).*

| Prediction system | 1/16° NLOM | 1/32° NLOM | 1/8° NCOM | 1/12° HYCOM | 1/32° NLOMn |
|---|---|---|---|---|---|
| Resolution at 20°N | 8 km | 4 km | 18 km | 8 km | No Assim |
| | % of eddies present in the model | | | | |
| All eddies | 70 | 90 | 55 | 80 | 35 |
| Large eddies, 1-10 | 80 | 100 | 80 | 90 | 20 |
| Small eddies, 11-20 | 60 | 80 | 30 | 70 | 50 |
| | Median eddy center position error, km | | | | |
| All eddies | 35.5 | 29 | 48 | 50 | 42 |
| Large eddies | 42.5 | 37 | 57 | 68 | 38 |
| Small eddies | 32.5 | 22.5 | 47 | 44 | 42 |

***Table 1:*** *Eddy depiction in ocean prediction models compared to SeaWiFS ocean color in the northwestern Arabian Sea and Gulf of Oman.*

***Notes to Table 1***

*The ocean color eddy ID numbers are plotted in Figure 5a. Eddies are numbered in order of decreasing size as depicted by the ocean color. Eddy position measurement error is 10–15 km in both the ocean color and the models.*

*1/32° NLOM: 1/32° global NLOM seven-layer prediction system with assimilation of altimeter track data from the ERS-2, GFO and Jason-1 altimeters (system presently operational at NAVOCEANO).*

*1/16° NLOM: Then operational 1/16° global NLOM seven-layer prediction system with assimilation of real-time altimeter track data from the ERS-2 and GFO altimeters (Jason-1 was not in the operational data stream at that time).*

*1/8° NCOM: 1/8° global NCOM 40-level prediction system with assimilation of 1/32° NLOM SSH via synthetic T & S profiles (presently operational at NAVOCEANO).*

*1/12° HYCOM: .08° global HYCOM prediction system with 32 hybrid layers and assimilation of altimeter track data from the ERS-2, GFO and Jason-1 altimeters plus T & S profiles (presently pre-operational and running in real time at NAVOCEANO).*

*1/32° NLOMn: 1/32° global NLOM with no assimilation of ocean data, only atmospheric forcing.*

*Adapted from Shriver et al. (2007) and Hurlburt et al. (2008a). See those references for more information.*

The role of ocean model dynamical interpolation skill in mapping the eddies is illustrated in Figure 5g,h,i using the prediction system with the highest horizontal resolution (4 km). These panels illustrate the evolution of the nowcast at one-week intervals. Figure 5i is the same as 5c except that all the altimeter tracks from ERS-2 (in red), GFO (black) and Jason 1 (white) crossing the region are overlaid. The tracks observed during the week ending with the nowcast date are overlaid as solid lines and the remainder as dashed lines. To illustrate the role of model dynamical interpolation skill, we will focus on a particular current system and associated eddies 2, 12, and 13. In the ocean color image the current system is seen entering the region as a ribbon of low chlorophyll near 60°E. This current flows northward to ~18°N where it bifurcates into an eastward branch that wraps around anticyclonic eddy 2 and a branch that flows westward just north of 18°N to ~58.5°E. There it turns northward and subsequently wraps around cyclonic eddy 12. Eddy 12 and the adjacent anticyclonic eddy 13 form a counter-rotating vortex pair. All three of the eddy-resolving prediction systems (Fig. 5b,c,e) depict this entire complex of currents and eddies, with greatest accuracy in the prediction system with the highest horizontal resolution (Fig. 5c). The eddy-permitting system (Fig. 5d) represents the inflowing current and the branch that wraps around large eddy 2, but the remainder of the current and eddy complex is poorly

represented. None of it is depicted in the atmospherically-forced simulation without ocean data assimilation (Fig. 5f).

On 22 Sept. (Fig. 5g) the inflow along ~60°E and eddy 12 are already present, but the remainder of the complex is quite different from 6 Oct. (Fig. 5i). There is no bifurcation of the inflowing current and no eddy 13, only anticyclonic flow around a zonally-oriented SSH ridge with a weak and amorphous version of eddy 2 near the eastern end. The inflowing current and the westward extension of the ridge are quite well observed by satellite altimetry, but eddy 12 is only peripherally observed. By 29 Sept. the westward extension of the ridge has weakened greatly (observed by one GFO altimeter track) and eddy 2 has strengthened. Again eddy 12 is only peripherally observed and eddy 13 still has not formed. The bifurcation of the inflowing current near 18°N is in the early stages of development in a region not observed by altimetry. The development of the bifurcation and eddy 13 occur during the week leading up to 6 Oct., the date shown in Figure 5 a-f. However, none of this development was observed by altimetry and none of the current/eddy system west of the inflowing current near 60°E was observed by the altimetry during that week. This example illustrates the importance of ocean model dynamical interpolation skill in the data assimilation and its role in extending the ability to map the mesoscale to small eddies. Further, all three of the eddy-resolving prediction systems (Fig. 5 b, c, e) represented this entire complex current and eddy system (while the non-assimilative model represented none of it). Therefore, this is not just an extremely fortuitous result.

## 6. Exploring the time scale for ocean weather prediction skill

In Figure 6 we investigate the feasibility of forecast skill on time scales up to a month, well beyond the ~ one week time scale for atmospheric predictive skill. Figure 6a-f from 1/12° global HYCOM illustrates forecast skill over the global ocean (in the latitude range 45°S-45°N) and in several subregions, including a region (Fig. 6c) similar to that used in Figure 5. In each panel three forecasts are verified using anomaly correlation between forecast SSH and the final and best nowcast performed 5 days in arrears. The green line shows anomaly correlation when analysis quality atmospheric forcing is used throughout the forecast, the red line when the atmospheric forcing reverts toward climatology after 5 days (termed operational forcing), and the blue line represents a forecast of persistence (a forecast of no change). In 5 regions (Fig. 5a-e) the forecast skill (anomaly correlation > .6) extends well beyond the time scale for atmospheric prediction skill and is only moderately degraded by the use of operational forcing. The Yellow and Bohai Seas are a notable exception. In that region a forecast of persistence loses skill in less than two days. Skill is also rapidly lost when the atmospheric forcing reverts toward climatology. However, the anomaly correlation remains very high as long as analysis quality forcing is used.

Hurlburt et al. (2008a) discuss ocean prediction skill in relation to classes of response to atmospheric forcing. The Yellow and Bohai Seas are very shallow. In shallow water and the surface mixed layer (e.g. sea surface temperature (SST) and mixed layer depth) the ocean responds rapidly to the atmospheric forcing and the forecast rapidly becomes more sensitive to the atmospheric forcing than the initial state.

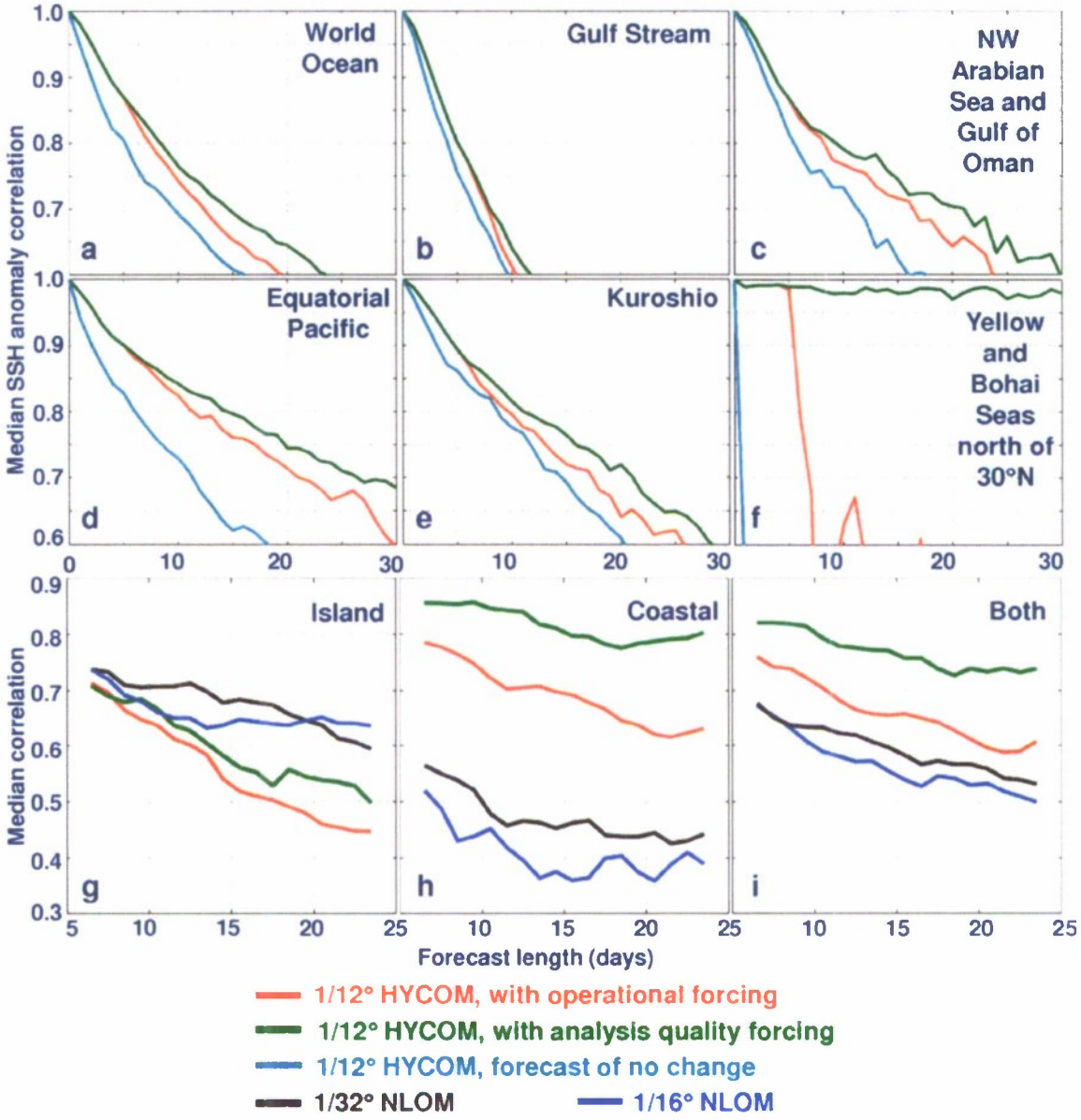


***Figure 6:*** *Verification of 30-day ocean forecasts, (a-f) median SSH anomaly correlation of HYCOM forecasts versus forecast length in comparison with the verifying analysis for (a) the global domain (45°S–45°N) and five subregions (b-f). The red curves verify forecasts using operational atmospheric forcing which reverts toward climatology after five days. The green curves verify "forecasts" with analysis-quality forcing for the duration, and the blue curves verify forecasts of persistence (i.e., no change from the initial state). The plots give median statistics over twenty 30-day forecasts initialized during the period from January 2004 through December 2005, a period when data from three nadir-beam altimeters were assimilated. The same HYCOM forecasts and twenty-two 30-day NLOM forecasts from June, 2001 – June 2002 were used to obtain (g-i) median correlation between forecast and observed SSH fluctuations from 1/12° HYCOM with operational forcing during the forecast (red lines), 1/12° HYCOM with analysis quality forcing for the duration (green lines), 1/16° (blue lines), and 1/32° (black lines) NLOM (both with operational atmospheric forcing) at (g) 23 (49) open ocean island tide gauge stations for HYCOM (NLOM), (h) 91 (29) coastal tide gauges for HYCOM (NLOM), and (i) all 114 (78) tide gauges for HYCOM (NLOM). A 13-day moving average was applied to filter time scales not resolved by the altimeter data. Tide gauge SSH data are not assimilated by the ocean prediction systems. Results are adapted from Hurlburt et al. (2008a) and Shriver et al. (2007).*

In contrast, mesoscale variability in the deep ocean is largely nondeterministic in relation to atmospheric forcing due to flow instabilities. Thus, the time scale for predictive skill is more dependent on the quality of the initial state, the accuracy of the model dynamics, and the time scale of the flow instabilities than on the atmospheric forcing. The Gulf Stream is particularly difficult to forecast and the 10-day Gulf Stream forecasts from Mercator Océan (Fig. 3) are right at the limit for useful forecast skill in HYCOM (Fig. 6b). Earlier we identified some shortcomings in 1/12° global HYCOM and Mercator Océan dynamics and simulation skill in the Gulf Stream region (without ocean data assimilation). Would improvements yield improved forecast skill in the region? Hurlburt and Hogan (2000, 2008) show that 1/32° (3.5 km resolution) NLOM (without ocean data assimilation) demonstrates more realistic dynamics and increased simulation skill in the Gulf Stream region based on extensive model-data comparisons. Correspondingly, the 1/32° global NLOM prediction system yields ~15-day forecast skill in the Gulf Stream region (Hurlburt et al., 2008a). Since HYCOM and Mercator Océan are inherently more accurate in ocean model design, there is opportunity for even greater increases in Gulf Stream region forecast skill, when their full potential in realized.

There are significant pitfalls in using model nowcasts to verify model forecasts. For example, decreases in input data could lead to apparent increases in forecast skill because the evolution of the nowcast was less constrained by data. In addition, coarser resolution models could demonstrate greater forecast skill than finer resolution models because of smoother, larger scale features that became out of phase more slowly. However, in these models persistence would generally have greater skill and the spread between the forecast and persistence for a given forecast length would be smaller. Therefore, when prediction system resolution is increased, an increased difference between the anomaly correlation of the forecast and the (lower) anomaly correlation of persistence is a better indicator of increased forecast skill than the anomaly correlation of the forecast alone (Shriver et al., 2007).

The preceding pitfalls also highlight the need to use independent, unassimilated data sets in assessing forecast skill. In Figure 6g, h, i unassimilated tide gauge data are used to assess model skill in forecasting SSH. For this purpose forecast skill is assessed against island and coastal stations separately, as well as combined. HYCOM forecasts with both analysis quality forcing (green lines) and operational forcing (red lines) are assessed. In addition, 1/16° (blue lines) and 1/32° (black lines) NLOM forecasts with operational forcing are assessed. A 13-day moving average was applied to the SSH time series to filter time scales not resolved by the altimeter data. Analysis quality forcing has much greater impact on forecast skill at the coastal stations than the island stations, as expected based on the earlier discussion. At the coastal stations the NLOM forecasts are clearly inferior to the HYCOM forecasts because NLOM does not include shallow water or shallow water dynamics and the nearest HYCOM grid point is generally closer to the coastal tide gauge than the nearest NLOM grid point. At the island stations the NLOM forecasts appear to have an edge over HYCOM, but different time periods and some different tide gauges were used in assessing HYCOM and NLOM forecast skill, so only large differences are meaningful. In both cases the 1/32° NLOM forecasts generally outperform the 1/16° NLOM forecasts.

## 7. Forecasting of sea surface temperature (SST) using eddy-resolving ocean models

In the future it is likely that global ocean prediction systems will become components of earth system prediction models (coupled atmosphere, ocean, ice, surface wave, land, and hydrological models) to greatly expand the predictive capability for the earth's environment and increase the time scale for useful predictive skill.

Therefore accurate nowcasting and forecasting of SST is a particularly crucial capability for global ocean prediction models. Eddy-resolving global ocean prediction systems are advantages for this application because of their ability to accurately map sharp ocean fronts and resolve the response to hurricanes and regions of coastal upwelling. Figure 7 presents an assessment of 1/12° daily week-long SST forecasts by Mercator Océan with forcing from ECMWF atmospheric forecasts. After one day the error is small over most of the domain but relatively large along the Gulf Stream, a region with large SST gradients and high variability. After one week relatively large error tends to be found along coastlines and in the region of equatorial Atlantic upwelling. Upwelling is also prevalent in the area of large error just to the north along the coast of Africa (as well as other regions). The area of large SST error in the open Atlantic around 60°W, 30°N

is the consequence of a hurricane and error in the hurricane forecast track. Figure 7c shows that overall the error in the SST forecasts is quite small and the forecasts are clearly superior to a forecast of persistence, the present approach used for SST in atmospheric forecast models.

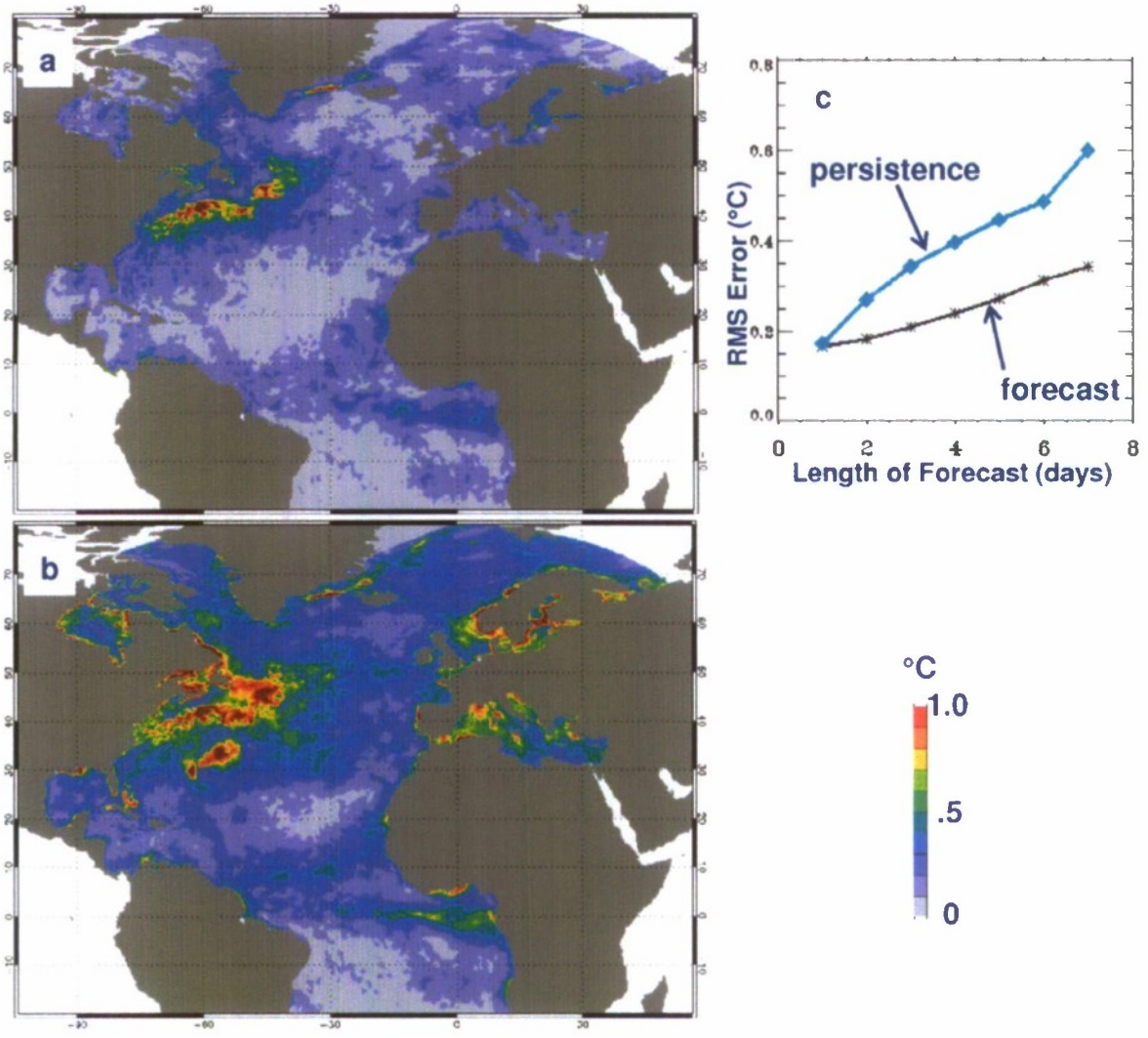


***Figure 7**: Spatial distribution of rms error for (a) the 1-day and (b) the 7-day 1/12° operational Mercator Océan SST forecasts. The time evolution of the SST error growth in comparison to persistence is shown in (c). The statistics were computed from the forecasts over the 4-month time period June-Sept. 2008.*

## 8. Coastal region prediction using large-scale eddy-resolving ocean prediction systems

Another important attribute of eddy-resolving global and basin-scale ocean models is their ability to provide useful resolution in coastal regions. These are generally the regions of greatest interest to prediction system users. In addition, the eddy-resolving large scale models play an essential role in providing boundary conditions to even higher resolution regional and coastal models. Here we use results from the Australian global BLUElink system to illustrate the ability of an eddy-resolving prediction system to represent an observed coastal upwelling event and to nowcast and forecast coastally trapped waves along the coast of Australia.

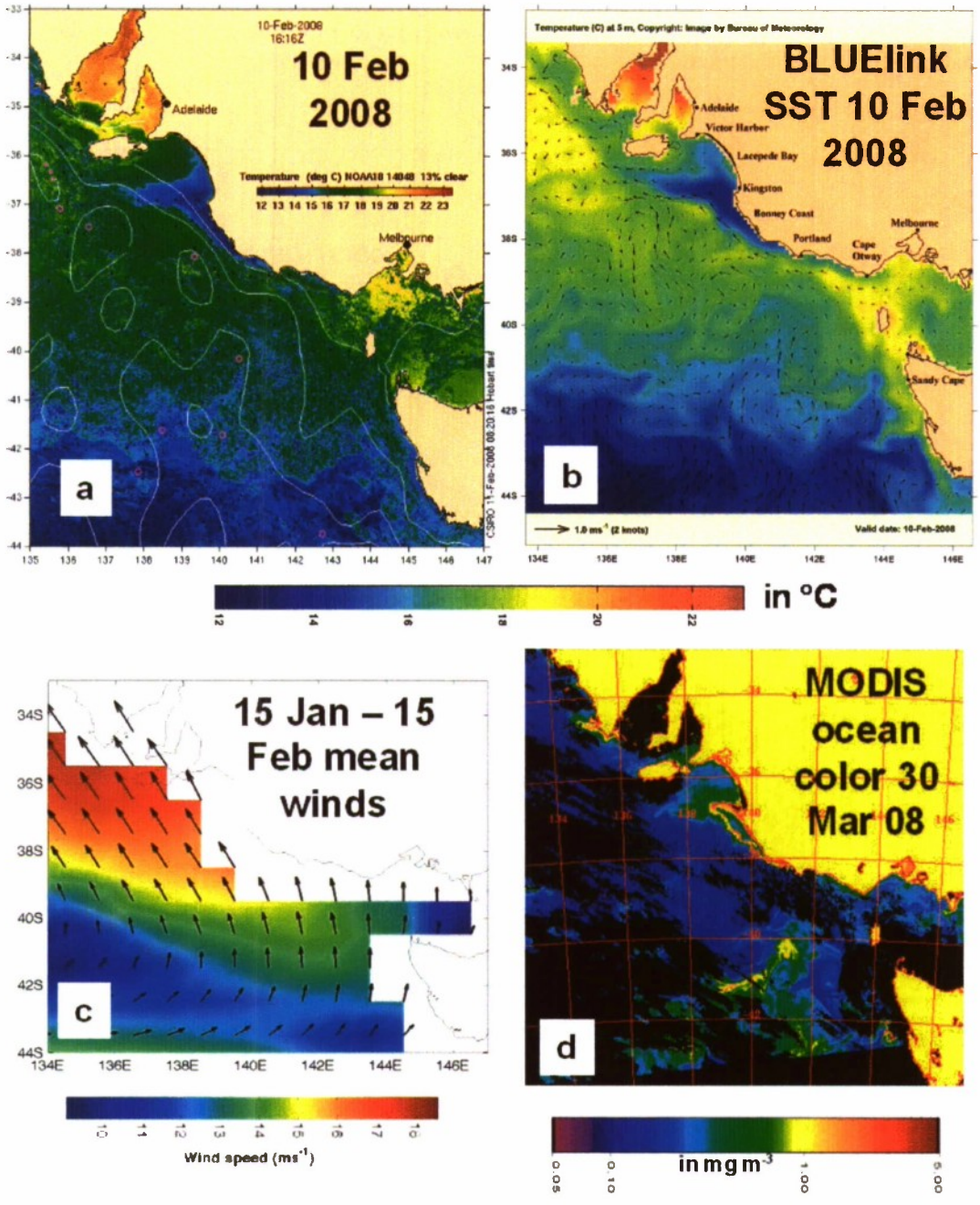


***Figure 8:*** *Depiction of a strong coastal upwelling event off southern Australia. (a) Observed SST from AVHRR on 10 Feb 2008 with a model-independent analysis of SSH from satellite altimeter data (white contours) and related geostrophic currents (black arrows) overlaid, (b) BLUElink SST and current vectors for 10 Feb 2008, (c) mean 15 Jan – 15 Feb 2008 winds from the QuikSCAT scatterometer, and (d) MODIS ocean color on 30 Mar 2008.*

Figure 8 depicts a very strong upwelling event on the South Australian coast between Adelaide and Melbourne, (a) as observed in SST from satellite AVHRR (near 37°S, 138°-140°E) and (b) as depicted in BLUElink SST. This event was preceded by a month of upwelling-favorable winds (Fig. 8c) and demonstrated a strong impact on chlorophyll productivity more than a month later (Fig. 8d). One might argue that since BLUElink assimilated SST, depiction of the upwelling event is superficial, but that is clearly not the case. A model-independent analysis of SSH from satellite altimetry (white lines overlaid on Figure 8a) and associated geostrophic currents (black arrows) show no influence from the upwelling event, but the

BLUElink currents (arrows in Figure 8b) are strongly influenced by the upwelling. This example illustrates the importance of atmospheric forcing as a data type in the ocean nowcast, an example where the ocean model transformed the atmospheric forcing into a realistic oceanic response.

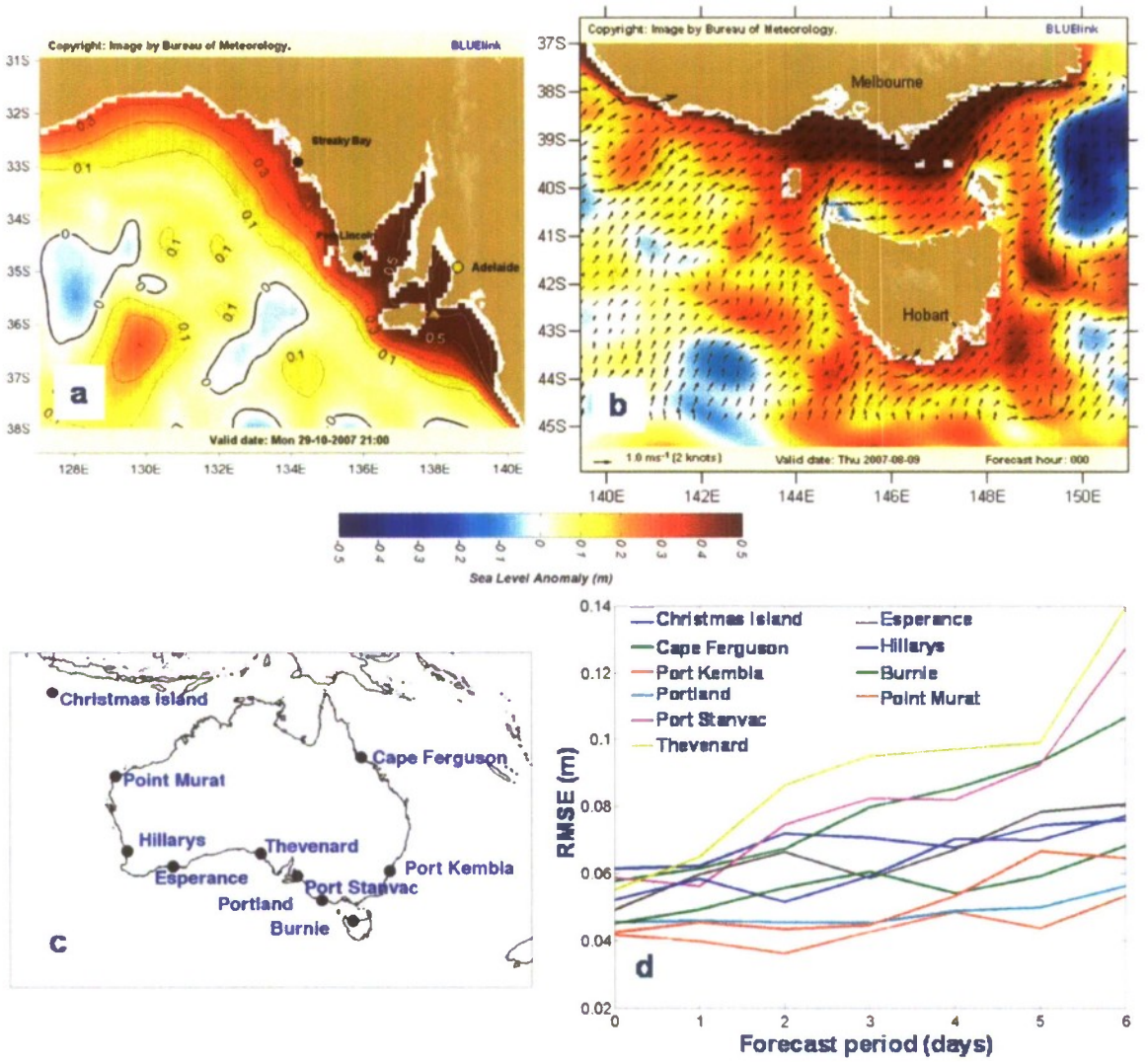


***Figure 9**: (a,b) Operational BLUElink snapshots of two different coastally trapped waves propagating eastward along the south coast of Australia on (a) 29 Oct. 2007 and (b) 9 Aug. 2007. (a) depicts SSH and (b) depicts SSH with current vectors overlaid. (c) marks the locations of ten tide gauge stations used in verifying (d) nowcasts (day 0) and 6-day forecasts of coastally trapped waves.*

Figure 9 illustrates the impact of two coastally trapped waves on SSH and currents near the coast, as they propagate eastward along the south coast of Australia (Fig. 9a,b). Again these features are largely initiated by the atmospheric forcing. Figure 9b is particularly interesting because it illustrates the bifurcation of a coastally trapped wave as it reaches the Bass Strait, which separates the Australian mainland and the island of Tasmania. The Bass Strait is shallow and the portion of the wave propagating in shallow water passes through the strait while the portion lying over deep water, farther offshore, passes South of Tasmania. These coastally trapped waves can have significant impacts and the Australian Bureau of Meteorology is using the BLUElink system to maintain a monitoring and forecast capability for these features that is verified by 10 tide gauge stations around Australia (Fig. 9c). Nowcast (day 0) and forecast verification statistics up to 6 days at these 10 stations are shown in Figure 9d.

## 9. Summary and Conclusions

The feasibility of global high resolution analyses and forecasts at the mesoscale was illustrated by demonstrating several key capabilities. The first was a demonstration of eddy-resolving global ocean modeling without ocean data assimilation, because an eddy-resolving model is a key component of a global prediction system for mesoscale ocean features, a point repeatedly verified in subsequent examples. Nowcasting and forecasting of mesoscale variability by assimilation of satellite altimeter data is a key capability demonstrated in multiple examples, including (1) the capability to verify specific mesoscale features using independent data, (2) the ability of eddy-resolving ocean models to accurately map smaller eddies than can be mapped in model-independent analyses, and (3) an exploration of the time scale for oceanic predictive skill in different dynamical regimes. Forecast skill on time scales up to about one month was demonstrated for mesoscale variability. Using forecast atmospheric forcing, forecast skill of at least one week was demonstrated for sea surface temperature. That is an essential capability for future coupled ocean-atmosphere prediction. Finally, nowcast/forecast skill was demonstrated in coastal regions for a coastal upwelling event and for coastally trapped waves. That capability is especially important for user applications and for nested coastal models with even higher resolution.

## Acknowledgements

The U. S. component is a contribution to the project, U. S. GODAE: Global Ocean Prediction with the HYbird Coordinate Ocean Model (HYCOM), funded under the National Ocean Partnership Program (NOPP). The U. S. effort was also supported by grants of computer time from the U. S. Defense Dept. High Performance Computing Modernization Program (HPCMP). The European high resolution global ocean system was developed by Mercator Océan with the financial support of the European Mersea integrated project for the development, validation, and exploitation of the system and from the Région Midi Pyrénées, which financed a dedicated computer for this project. The BLUElink science and technical team was supported by the Bureau of Meteorology, CSIRO, Wealth from Oceans National Research Flagship, and the Royal Australian Navy. The Australian, French and USA groups have all been active participants in GODAE and GODAE has contributed greatly to the success of their global ocean prediction system development efforts.

### References

Brasseur, P. and J. Verron (2006) The SEEK filter method for data assimilation in oceanography: a synthesis. *Ocean Dynamics*, **56**: 650-661.

Bryan, F. O., M. W. Hecht, and R. D. Smith (2007) Resolution convergence and sensitivity studies with North Atlantic circulation models. Part I. The western boundary current system. *Ocean Model.*, **16**: 141-159.

Chassignet, E. P. and D. P. Marshall (2008) Gulf Stream separation in numerical ocean models. In: Hecht, M. W. and H. Hasumi (Eds.), *Ocean Modeling in an Eddying Regime,* Geophysical Monograph **177**. American Geophysical Union, Washington, D.C., 39-61.

Cummings, J., L. Bertino, P. Brasseur, I. Fukumori, M. Kamachi, M. Martin, K. Mogensen, P. Oke, C.E. Testut, J. Verron, and A. Weaver (2008) Ocean data assimilation systems for GODAE. *GODAE Final Symposium Proceedings,* 12-15 Nov. 2008, Nice, France.

Dombrowsky, E., L. Bertino, G. Brassington, E. Chassignet, F. Davidson, H. Hurlburt, M. Kamachi, T. Lee, M. Martin, S. Mei, M. Tonani (2008) GODAE systems in operation. *GODAE Final Symposium Proceedings,* 12-15 Nov. 2008, Nice, France.

Ducet, N., P. Y. Le Traon, and G. Reverdin (2000) Global high-resolution mapping of ocean circulation from TOPEX/Poseidon and ERS-1 and -2. *J. Geophys. Res.*, **105**(C8): 19,477-19,498.

Griffes, S. M., M. J. Harrison, R. C. Pacanowski, and A. Rosati (2004) A technical guide to MOM4. GFDL Ocean Group Technical Report No. 5, NOAA/Geophysical Fluid Dynamics Laboratory, 339 pp.

Harrison, D. E., M. Johnson, C. Clark, D. Roemmich, H. Freeland, G. Goni, M. Merrifield, M. McPhaden, R. Weller, U. Send, D. Meldrum, G. Ball, and M. Hood (2008) The in situ global ocean observing system – Progress since OceanObs 1999. *GODAE Final Symposium Proceedings,* 12-15 Nov. 2008, Nice, France.

Hurlburt, H. E. and P. J. Hogan (2000) Impact of 1/8° to 1/64° resolution on Gulf Stream model-data comparisons in basin-scale subtropical Atlantic Ocean models. *Dyn. Atmos. Oceans,* **32**: 283-329.

Hurlburt, H. E. and P. J. Hogan (2008) The Gulf Stream pathway and the impacts of the eddy-driven abyssal circulation and the Deep Western Boundary Current. *Dyn. Atmos. Oceans,* **45**: 71-101.

Hurlburt, H. E., E. P. Chassignet, J. A. Cummings, A. B. Kara, E. J. Metzger, J. F. Shriver, O. M. Smedstad, A. J. Wallcraft, and C. N. Barron (2008a) Eddy-resolving global ocean prediction. In: M. Hecht and H. Hasumi (Eds.), *Ocean Modeling in an Eddying Regime*, Geophysical Monograph **177.** American Geophysical Union, Washington, D. C., 353-381.

Hurlburt, H. E., E. J. Metzger, P. J. Hogan, C. E. Tilburg, and J. F. Shriver (2008b) Steering of upper ocean currents and fronts by the topographically constrained abyssal circulation. *Dyn. Atmos. Oceans,* **45**: 102-134.

Lumpkin, R. and M. Pazos (2007) Measuring surface currents with SVP drifters: The instrument, its data, and some recent results. In A. Griffa, A.D. Kirwan, A.J. Mariano, T. Özgökmen and T. Rossby (Eds.), *Lagrangian Analysis and Prediction of Coastal and Ocean Dynamics*, Cambridge Univ. Press, New York, 39-67.

Madec, G. (2008) "NEMO ocean engine". Note du Pole de modelisation, Institut Pierre-Simon-Laplace (IPSL), France, No. 27 ISSN No. 1288-1619.

NOAA (2008) Program Plan for Building a Sustained Ocean Observing System for Climate. Office of Oceanic and Atmospheric Research Climate Program Office, Climate Observation Division, <http://www.oco.noaa.gov/docs/programplan_current.doc>

Oke, P. R., G. B. Brassington, D. A. Griffin, and A. Schiller (2008) The Bluelink ocean data assimilation system (BODAS). *Ocean Model.,* **21**: 46-70.

Shriver, J. F., H. E. Hurlburt, O. M. Smedstad, A. J. Wallcraft, and R. C. Rhodes (2007) 1/32° real-time global ocean prediction and value-added over 1/16° resolution. *J. Mar. Syst.,* **65**: 3-26.

Wilson, S., J. Benveniste, H. Bonekamp, C. Donlon, M. Drinkwater, J.-L. Fellous, B. S. Gohil, G. Jacobs, P.-Y. Le Traon, E. Lindstrom, L. Mingsen, K. Nakagawa, F. Parisot (2008) Satellite observing systems and relevance to GODAE. *GODAE Final Symposium Proceedings,* 12-15 Nov. 2008, Nice, France.